# In Vivo Imaging of Lymphocyte Trafficking

Cornelia Halin, J. Rodrigo Mora, Cenk Sumen, and Ulrich H. von Andrian

The CBR Institute for Biomedical Research and the Department of Pathology, Harvard Medical School, Boston, Massachusetts, 02115;
email: halin@cbr.med.harvard.edu; mora@cbr.med.harvard.edu; sumen@cbr.med.harvard.edu; uva@cbr.med.harvard.edu

Annu. Rev. Cell Dev. Biol.
2005. 21:581–603

First published online as a Review in Advance on June 29, 2005

The *Annual Review of Cell and Developmental Biology* is online at http://cellbio.annualreviews.org

doi: 10.1146/annurev.cellbio.21.122303.133159



1081-0706/05/1110-0581$20.00

## Key Words

intravital microscopy, two-photon microscopy, lymph node, immune response

## Abstract

Over the past decades, intravital microscopy (IVM), the imaging of cells in living organisms, has become a valuable tool for studying the molecular determinants of lymphocyte trafficking. Recent advances in microscopy now make it possible to image cell migration and cell-cell interactions in vivo deep within intact tissues. Here, we summarize the principal techniques that are currently used in IVM, discuss options and tools for fluorescence-based visualization of lymphocytes in microvessels and tissues, and describe IVM models used to explore lymphoid and non-lymphoid organs. The latter will be introduced according to the physiologic itinerary of developing and differentiating T and B lymphocytes as they traffic through the body, beginning with their development in bone marrow and thymus and continuing with their migration to secondary lymphoid organs and peripheral tissues.

## Contents



## INTRODUCTION

Over 40 years of research on leukocyte trafficking (Gesner & Gowans 1962) have generated substantial insights into the pathologic and physiologic trafficking patterns of blood-borne leukocyte subsets and their role in health and disease (Butcher & Picker 1996, Springer 1994, von Andrian & Mackay 2000). This knowledge has been essential for the recent development of new anti-inflammatory therapies, such as monoclonal antibodies against LFA-1 or alpha-4 integrins, to treat psoriasis and multiple sclerosis, respectively (Miller et al. 2003a, Vugmeyster et al. 2004). Among the established techniques to study leukocyte trafficking, direct observation by intravital microscopy (IVM) is the oldest. Unlike other in vivo techniques that study leukocyte accumulation in tissues at the population level, IVM can analyze migratory behavior at the single-cell level and pinpoint the role of traffic molecules in multistep intravascular adhesion cascades.

However, intravascular adhesion represents only one aspect of leukocyte trafficking; many leukocytes spend only a short part of their life in the blood. The circulation half-life of naïve T cells, for example, is ~30 min, whereas they spend hours to days migrating within secondary lymphoid organs (SLO), querying dendritic cells (DCs) for cognate antigen (Ag). The rules governing interstitial cell migration, the adhesion molecules, and chemoattractants that determine cellular tissue localization and dwell-time are still scarcely understood compared with the rules governing intravascular trafficking.

Our current knowledge about cellular tissue distribution or cell-cell interactions during immune responses stems largely from investigations employing histology or in vitro tissue assays. Until recently, technical difficulties associated with imaging of events within solid organs have limited IVM observations to membranous tissues or superficial regions of non-translucent organs. These constraints are now overcome by combining IVM with two-photon microscopy (2P-IVM) (Denk et al. 1990). 2P-IVM allows immune cell imaging in solid organs at depths of up to 500 $\mu$m below the surface without interfering with blood or lymph flow, tissue oxygenation, or innervation (Sumen et al. 2004). Results from 2P-IVM have radically altered our perception of cellular dynamics within SLO, e.g., by revealing a much more dynamic behavior of naïve T cells than would be predicted from their sessile appearance ex vivo. Additionally, two-photon microscopy (2PM) has extended the application of IVM to immunological research that reaches beyond trafficking. It is now feasible to observe immune response at subcellular resolution in situ (Sumen et al. 2004).

In addition to advances in photonics, IVM has gained momentum recently by innovations in other areas; the availability of refined fluorescent probes, improved hardware and software for three-dimensional image analysis, and a diverse array of drugs, antibodies,

recombinant proteins, and gene-targeted mice have contributed to the increasing acceptance and utilization of IVM as a powerful instrument for immunological research.

## MODES OF VISUALIZATION

The first intravascular IVM studies of leukocytes employed brightfield microscopy (BFM) dating back to the 19th century (Cohnheim 1889, Wagner 1839). In BFM, white light illuminates the background behind a tissue, which must be sufficiently translucent, such as the frog mesentery and tongue (Cohnheim 1889), or rodent mesentery and cremaster muscle (Atherton & Born 1972, Baez 1973). BFM cannot distinguish different leukocyte subpopulations, and analysis of leukocyte behavior is largely limited to intravascular cells because leukocytes are difficult to track in the extravascular space.

Epifluorescence IVM (EF-IVM) is best-suited to study intravascular lymphocyte adhesion because it allows visualization of distinct leukocyte subpopulations in solid organs (**Table 1**). Typically, EF-IVM employs long, working-distance, water-immersion objectives for close access to surgically exposed tissues submerged in a physiologic buffer. To reduce phototoxicity and photobleaching, microscopes can be equipped with video-triggered xenon-arc stroboscopes that generate microsecond-pulsed excitation light and substantially reduce light exposure (30,000-fold versus continuous illumination). Most intravascular adhesion events occur within

**Table 1 Murine IVM models employed for studying lymphocyte trafficking**

| Process | Organ | Imaging modality | Reference |
|---|---|---|---|
| Progenitor cell homing | BM | EFM | (Mazo et al. 1998) |
| Homing to SLO | Inguinal LN | EFM | (von Andrian 1996) |
| | Mesenteric LN | EFM | (Grayson et al. 2003) |
| | Peyer's Patch | EFM | (Bargatze et al. 1995) |
| | Spleen | EFM | (Grayson et al. 2003) |
| Migration within LN | Inguinal LN | 2PM | (Miller et al. 2003b) |
| | Popliteal LN | 2PM | (Mempel et al. 2004) |
| Inflammation and Immuno-surveillance | BM | 2PM | (Mazo et al. 2005) |
| | CNS (spc) | EFM | (Vajkoczy et al. 2001) |
| | CNS (cwm) | EFF | (Yuan et al. 1994) |
| | CNS (brain) | EFM | (Piccio et al. 2002) |
| | Cremaster– Muscle | BFM | (Baez 1973) |
| | | EFM | (Singbartl et al. 2001) |
| | Eye (iris) | EPF | (Becker et al. 2000) |
| | Intestine | EFM | (Massberg et al. 1998) |
| | | EPF | (Fujimori et al. 2002) |
| | Liver | EFM | (Nakagawa et al. 1996) |
| | | LSCM | (Hoffmeister et al. 2003) |
| | Pancreas | EFM | (Enghofer et al. 1995) |
| | Skin (ear) | EFM | (Reus et al. 1984) |
| | Skin (dsc) | EFM | (Lehr et al. 1994) |
| | Pancreas | EFM | (Enghofer et al. 1995) |
| | Tumor | EFM | (Leunig et al. 1992) |

Abbreviations: EFM, epifluorescence microscopy; CFM, confocal microscopy; BFM, brightfield microscopy; 2PM, 2-photon microscopy; LSCM, laser-scanning fluorescent microscopy; spc, spinal cord; cwm, cranial window model; dsc; dorsal skinfold chamber.

seconds (or faster) and are analyzed off-line from two-dimensional recordings taken at video frame rates [30 fps in NTSC (National Television System Committee)]. The principles of intravascular IVM and associated measurement parameters are summarized in **Figure 1*a*** and **Table 2**, respectively.

Although EF-IVM works well for superficial intravascular two-dimensional imaging, it is less suitable for deep tissue imaging. Nonconfocal EF-IVM below a sample's surface suffers from out-of-focus fluorescent signals, which reduce image quality and limit tissue penetration. Moreover, whereas blood flow dictates the directionality of cell movement in microvessels, extravascular cells can migrate freely in any direction, therefore requiring accurate three-dimensional tracking. The three-dimensional resolution needed to study interstitial cell behavior is not achievable with conventional fluorescence techniques. Confocal microscopy, which excludes out-of-focus fluorescence, was used successfully to generate three-dimensional images (see **Figure 1*b***for a schematic illustration). In intact lymph nodes (LN), confocal microscopy penetrates up to 80 $\mu$m deep, but cannot reach regions below the superficial cortex (Stoll et al. 2002). Recently, 2P-IVM has overcome many limitations of EF-IVM and confocal approaches (Denk et al. 1990). By generating interpretable images at $\leq$500 $\mu$m depth (**Figure 2**), 2P-IVM can visualize cell migration and cell-cell interactions in regions that were previously inaccessible. Technical aspects of 2P-IVM were reviewed recently (Cahalan et al. 2002, Sumen et al. 2004, Zipfel et al. 2003); measurement parameters to quantify cell migration from three-dimensional data sets are summarized in **Table 2**.

## FLUORESCENT TAGS AND LABELS

IVM relies on tools, such as fluorescent compounds or proteins, for visualizing cell populations with high specificity, without altering their phenotype or function. Countless IVM experiments have used reagents such as rhodamine 6G or acridine red or orange, which, upon i.v. injection, accumulate in leukocytes (and to some extent in other cells), but not in red cells. A drawback to this approach is the potential excitation light-induced phototoxic effect that alters hemodynamics and cell adhesion (Saetzler et al. 1997). This issue can be partly alleviated by video-triggered xenon-arc stroboscopes (discussed above). One method for studying distinct leukocyte subsets consists of purifying cells from donor mice, labeling them fluorescently in vitro and re-injecting them into a recipient. Aside from the multitude of organic fluorophores, an interesting recent addition to the fluorescence tool box are the nanometer-scale semiconductor crystals called quantum dots, which emit in different colors (400–1350 nm), are photostable, and are bright enough for detection of single particles (Michalet et al. 2005).

Transgenic mice expressing green fluorescent protein (GFP) or its variants in a cell type-specific fashion are alternatives to ex vivo purified, fluorescently labeled cells. This approach subjects cells to less ex vivo handling (see "Technical Considerations," above), and genetically encoded fluorescent tags do not become diluted or fade in dividing cells. Additionally, $GFP^+$ transgenic leukocytes can be studied endogenously without ex vivo manipulation or adoptive transfer (Lindquist et al. 2004, Manjunath et al. 1999, Singbartl et al. 2001, Weninger et al. 2003). Alternatively, some cell populations can be specifically labeled in situ. For example, dermal DCs and Langerhans cells (LC) take up intracutaneously injected carboxy-fluorescein diacetate succinimidyl ester (CFSE) within tissues and subsequently migrate to draining LN where they can be imaged (Miller et al. 2004b).

Recently, GFP-like green, yellow, and red fluorescent proteins have been cloned (Matz et al. 1999), notably DsRed, a red fluorescent protein from Discosoma coral. Red light penetrates tissues better than green fluorescence,

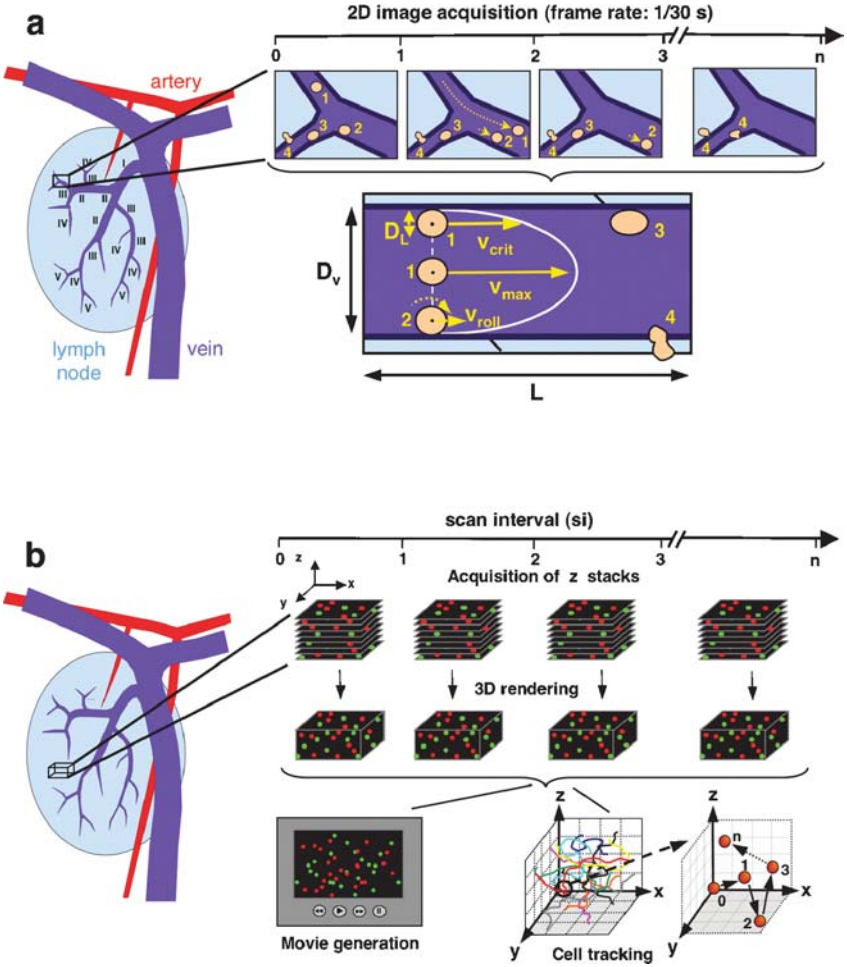


**Figure 1**

Principles of video-based IVM to analyze intravascular trafficking events and interstitial MP-IVM for two-dimensional recordings. Schematic representations of a murine LN with a typical venular tree (*a*, *b*, *left*). Venular order designations (in *a*) are assigned (Roman numerals) by counting successive generations of venular branches in upstream direction from the collecting venule draining into the larger vein. (*a*, *right*) Schematic representation of a vessel as seen in successive video frame segments (1, 2, 3. . .n). The different modes of intravascular cellular trafficking are illustrated by free flowing (1), rolling (2), sticking (3), and diapedesing (4) cells. The lower panel depicts the fluid dynamic parameters that determine leukocyte velocities in microvessels with laminar blood flow. For further definitions of each parameter refer to **Table 2**. (*b*, *right*) Schematic representation of the three-dimensional image acquisition process employed in confocal or MP-IVM. Stacks of optical sections are acquired by rapid incremental vertical repositioning of the objective along the *z* axis. In the example shown, one *z* stack is composed of eight sections at defined focal depths that are acquired during one scan interval (si). Image acquisition of *z* stacks is continuously repeated over a certain time period (si 1 → n). Each *z* stack is subsequently processed by image analysis software and rendered as a three-dimensional volume. Movies are typically generated as two-dimensional projections of successive three-dimensional image stacks. Using image analysis software, tracking identities are assigned to individual cells to follow their paths over time. The position of the tracked cell's centroid yields a series of *xyz* coordinates that correspond to different imaging time points. Detailed explanations of intravascular and interstitial measurement parameters are provided in **Table 2**.

**Table 2 Measurement parameters used in intravascular and interstitial IVM**

| | Description | Unit |
|---|---|---|
| **Intravascular 2D IVM** | | |
| Vascular dimensions: diameter ($D_v$), length ($L$) | Best determined after injection of a fluorescent plasma marker, e.g., 150 kD FITC dextran; $L$ = distance of unbranched vascular segment between bifurcations | $\mu$m |
| Luminal surface area ($A$) | $A = (D_v/2)^2 * \pi * L$ | $\mu m^2$ |
| Maximal velocity ($v_{max}$) | Velocity of the fastest flowing cell in a population of non-interacting cells, assumed to be flowing in the centerline | $\mu$m/s |
| Mean blood flow velocity ($v_{blood}$) | Calculated from velocity analysis of non-interacting cells assuming a parabolic flow profile: $v_{blood} = v_{max}/(2 - (D_l/D_v)^2)$, where $D_l$ = leukocyte diameter (7 $\mu$m) | $\mu$m/s |
| Blood flow ($Q$) | $Q = v_{blood} * \pi * D_v{}^2/4 * 10^{-6}$ | nl/s |
| Critical velocity ($v_{crit}$) | The lowest velocity that a non-interacting cell can assume in a microvessel. Can be estimated as $v_{crit} = v_{max} * (D_l/D_v) * (2 - (D_l/D_v))$, where $D_l$ = leukocyte diameter (7 $\mu$m) | $\mu$m/s |
| Total cellular flux ($TF$) | Number of cells that pass a vessel during an observation period | $min^{-1}$ |
| Rolling | Cellular movement ($v_{roll}$) along the vessel wall that is detectably slower than $v_{crit}$ | |
| Rolling flux ($RF$) | Number of cells that roll in a vessel during an observation period | $min^{-1}$ |
| Rolling fraction ($RFx$) | Percentage of cells that roll in a vessel relative to the total cellular flux: $RFx = RF/\mathrm{TF} * 100$ | % |
| Sticking | Cellular arrest for ≥30 s in a physiologically perfused vessel | |
| Sticking flux ($SF$) | Number of cells that stick during an observation period | $min^{-1}$ |
| Sticking cell accumulation | $SF/A$ | $\mu m^{-2}$ |
| Sticking fraction ($SFx$) | Percentage of rolling cells that arrest in a vessel for ≥30 s: $SFx = SF/RF * 100$ | % |
| Sticking efficiency ($SFe$) | Percentage of cells that arrest in a vessel for ≥30 s relative to the total cellular flux: $SFe = SF/TF * 100$ | % |
| **Interstitial 3D IVM** | | |
| Instantaneous velocity (v) | Velocity measured during a defined time interval (t), e.g., $v_{0\to1} = d_{0\to1}/t_{0\to1}$ | $\mu$m/min |
| Mean velocity (V) | Mean velocity of a cell over the entire measurement period e.g., $V_{0\to n} = (v_{0\to1} + v_{1\to2} + v_{2\to3} + \ldots v_{n-1\to n})/n$ | $\mu$m/min |
| Displacement (d) | Distance between first and last imaging point e.g., $d_{0\to n} = \mathrm{sqrt}(\Delta x_{0\to n}{}^2 + \Delta y_{0\to n}{}^2 + \Delta z_{0\to n}{}^2)$ | $\mu$m |
| Mean Displacement (MD) | Average distance migrated from arbitrary points of origin over a selected time (t) representing a multiple of the scan interval (si) e.g., $MD_{(t=1si)} = (d_{0\to1} + d_{1\to2} + d_{2\to3} + \ldots d_{n-1\to n})/n$; $MD_{(t=2si)} = (d_{0\to2} + d_{1\to3} + \ldots d_{n-2\to n})/(n-1)$; $MD_{(t=3si)} = (d_{0\to3} + \ldots d_{n-3\to n})/(n-2)$ | $\mu$m |
| Chemotactic index (CI) | A measure for the directionality of cell migration. Represents the ratio of the displacement (d) over the total path length e.g., $CI = d_{0\to n}/(d_{0\to1} + d_{1\to2} + d_{2\to3} + \ldots d_{n-1\to n})$ | no dimension |
| Turning angle | The angle at which a cell deviates from a straight line between subsequent measurement intervals | degree |

(*Continued*)

**Table 2 (*Continued*)**

| Interstitial 3D IVM | Description | Unit |
|---|---|---|
| Persistence time | Time during which a cell continues to migrate in the same direction before making a significant turn. For detailed explanation see Sumen et al. (2004) | min |
| Motility coefficient | A measure for a cell's propensity to move away from its point of origin, analogous to the diffusion coefficient of Brownian motion. For detailed explanation see Sumen et al. (2004) | $\mu m^2/min$ |



and its spectral separation from green emitters allows multicolor-imaging (Verkhusha & Lukyanov 2004). However, the propensity of DsRed to form aggregates plus the slow folding and maturation of the protein have hampered widespread use in IVM. Recently developed monomeric DsRed variants might solve these problems (Verkhusha & Lukyanov 2004).

Other interesting probes for IVM are fluorescent indicators of cell activation and/or signaling, particularly fluorescent proteins that redistribute intracellularly or change fluorescence intensity or color. Fluorescent reporters can also measure intracellular biochemical mediators or protease and kinase activities (Zhang et al. 2002). Similarly, fluorescent sensors that are based on FRET (fluorescence resonance energy transfer) hold promise for IVM. Furthermore, photoactivatable fluorescent proteins that either become fluorescent or undergo a color change upon UV illumination have been reported (Patterson & Lippincott-Schwartz 2004). The latter may become useful for photo-labeling cells during IVM for long-term tracking and/or subsequent isolation.

## IVM MODELS: WATCHING THE LIFE-LONG JOURNEY OF T AND B LYMPHOCYTES

To protect the body from pathogens, the immune system must cope with the complex and challenging task of directing the right cells to the right place at the right time. Immunologists have learned to distinguish different lymphocyte subsets by distinct surface markers, which are telltale signs of a cell's prior exposure to Ag, the context in which the Ag was encountered (if at all), and the prevalent immunological function of the cell (see Supplemental Material **Table 1**. Follow the Supplemental Material link from the Annual Reviews home page at **http://www.annualreviews.org**). Most subset-defining markers are surface receptors involved in cell-cell recognition, such as adhesion molecules and chemoattractant receptors used by lymphocytes to gain access to different anatomic compartments (von Andrian & Mackay 2000). To understand the immune system, one must not only determine how cells detect and respond to outside stimuli, but also consider where each subset is exposed to such stimuli and what tissues(s) are accessible to the responding cells. Below, we discuss IVM models to study lymphocyte trafficking to and within lymphoid and non-lymphoid tissues (**Table 1**).

### Bone Marrow: Cradle for Versatile Travelers

In the bone marrow (BM), hematopoietic stem cells (HSC) give rise to the various cell constituents of blood. Some BM-derived leukocytes then home quickly to other organs and tissues. However, the BM is not only a site of continuous unidirectional egress of blood cells and extravascular leukocytes; many circulating cells also (re-)enter the BM. The latter event has been documented for leukocytes such as naïve and memory T cells, memory B cells, plasma cells, and HSC (Sumen et al. 2004).

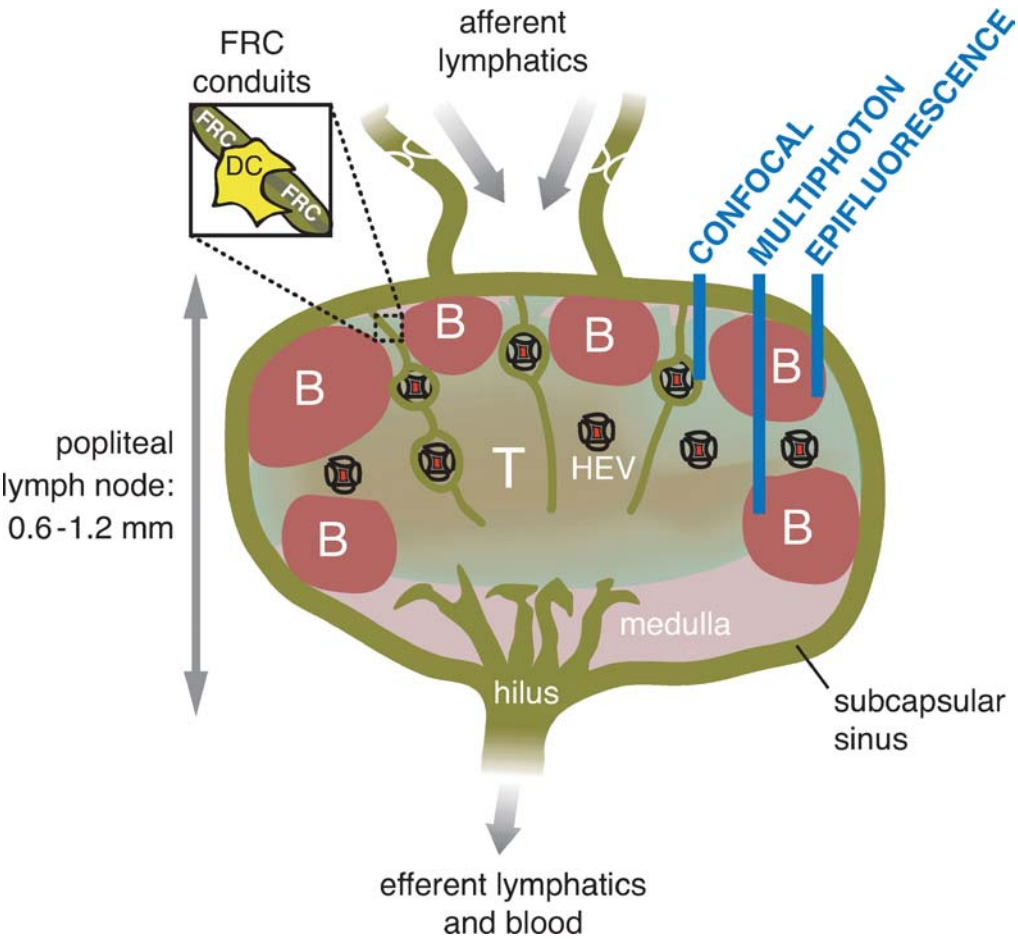


**Figure 2**

The lymph node. The diagram shows the distal B cell follicles and central T cell area of a schematized LN. Lymph flows into the node via the afferent lymphatics and courses around the node via the subcapsular sinus that surrounds the node. It can also flow into the medulla by traversing the cortex via the fibroblastic reticular cell (FRC) conduits that surround and interconnect a subset of high endothelial venules (HEVs), allowing sampling by resident DCs (*inset*). Lymph collects at the hilus and is removed from the node via the efferent lymphatic vessels. Approximate imaging depth for epifluorescence, confocal, and multiphoton imaging is also shown (murine popliteal lymph node).

The BM's inaccessible location has been a major obstacle for IVM: early studies in rabbit BM were performed over 30 years ago (reviewed in Mazo & von Andrian 1999), but technical challenges limited widespread application of this model. Recently, another technique for BM IVM was developed in mice (Mazo et al. 1998). This model exploits the fact that the bone covering BM cavities in the frontoparietal skull of mice is very thin and sufficiently transparent to visualize underlying BM. Thus only a small incision in the scalp is required, and the skull itself remains untouched. This model has been instrumental in analyzing adhesion events involved in homing of HSC (Katayama et al. 2003; Mazo et al. 1998, 2002) and central memory T cells (Mazo et al. 2005).

It is well established that the BM functions as a primary lymphoid organ, but recent reports suggest an additional role during primary and secondary T cell responses. The BM harbors naïve and memory T cells (Di Rosa & Santoni 2002), which are recruited from the blood (Koni et al. 2001, Mazo et al. 2005). Recent reports have established that the BM can support primary immune responses involving naïve T cells interacting with BM resident DCs (Feuerer et al. 2003, 2004). However, the BM can probably not support all types of adaptive immune responses, such as T cell–dependent antibody responses (Shinkura et al. 1996) or induction of allograft rejection (Lakkis et al. 2000). 2P-IVM may help reveal differences during T cell activation in BM versus SLO.

Distinct steps in lymphocyte differentiation are believed to take place within specialized supportive BM niches (Katsura 2002), but the microanatomic context of these events is unknown. HSC are concentrated in subendosteal regions within BM cavities (Calvi et al. 2003, Nilsson et al. 2001) and migrate to more central regions as they differentiate (Lord et al. 1975). This movement between niches is an active process that likely depends on attractants and stroma cells (Tokoyoda et al. 2004). 2P-IVM of skull BM offers a window to study the migration of lymphoid precursors. However, such studies require transgenic mice or transduced cells expressing fluorescent reporter genes under stage-specific promoters (Yu et al. 1999).

## Thymus: Essential Detour for T Cell Differentiation

BM-derived lymphoid progenitors migrate via the blood to the thymus where they develop into mature T cells (**Figure 3**). Little is known so far about the traffic molecules governing progenitor cell homing to the thymus, but thymocyte migration within the thymus has been studied. Static snapshots of thymocyte development were obtained by immunohistochemistry (Lind et al. 2001), which revealed that thymocytes migrate to special regions fostering successive developmental stages (Petrie 2003). Cell-cell interactions are critical for thymocyte development: Newly arranged T cell receptor (TCR) specificities of thymocytes are tested for their affinity for self-peptide-MHC complexes on thymic stromal cells during positive and negative selection.

The inaccessible location of the thymus in the thorax has so far impeded IVM in situ. Thymocyte differentiation in the medulla occurs $>500$ $\mu$m below the capsule, which complicates imaging by 2P-IVM. Given the absence of in vivo models, thymocyte behavior and motility have presently been visualized only in vitro, such as in fetal thymic organ cultures (FTOC), three-dimensional reaggregated thymic organ cultures (RTOC) (Bousso et al. 2002, Richie et al. 2002), or in fresh thymic slices (Bhakta et al. 2005). In these settings, thymocytes were highly motile and migrated along seemingly random trajectories similar to T cells in LN, albeit more slowly (Bhakta et al. 2005, Mempel et al. 2004). Bousso et al. analyzed thymocyte-stromal cell interactions by reaggregating fluorescent TCR transgenic $CD4^+CD8^+$ thymocytes with differentially labeled $MHC^{+/+}$ or $MHC^{-/-}$ stromal cells (Bousso et al. 2002). MHC recognition during positive selection led to prolonged thymocyte-stromal cell interactions. Both short, highly dynamic interactions and long-lived stable contacts were observed. The meaning of this behavior is presently unclear, but is reminiscent of the first two phases of T cell-Ag presenting DC interactions in LN (Mempel et al. 2004).

## Secondary Lymphoid Organs: Elementary School for Lymphocyte Activation and Differentiation

Once B and T cells have become fully differentiated in the BM and thymus, respectively, they embark on a relentless search for "their"

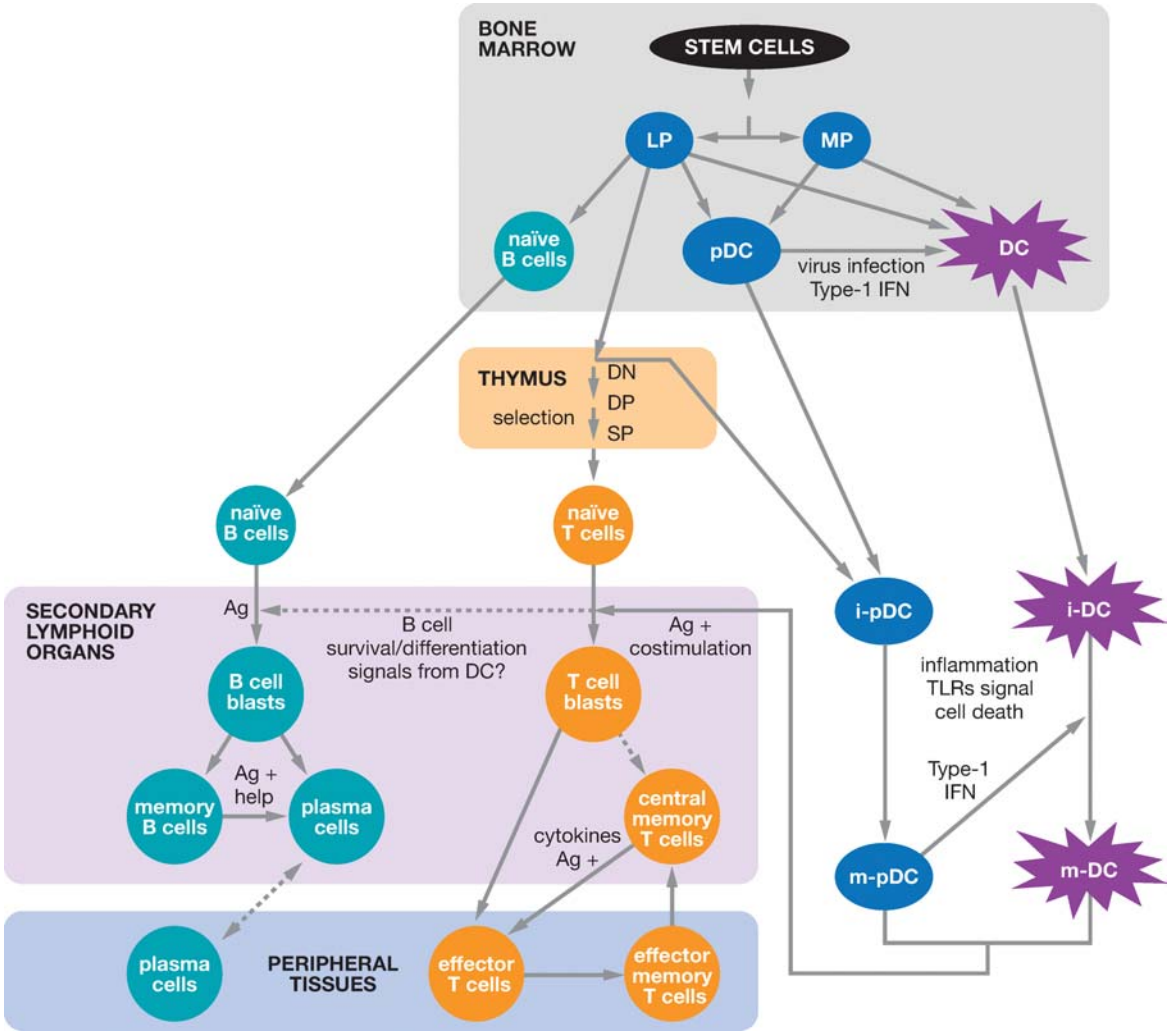


**Figure 3**

T cells, B cells, and dendritic cells: Lineage relationship, phenotype, and function. A common lymphoid progenitor (LP) gives rise to T cell precursors and B cells. T cell precursors undergo essential differentiation steps in the thymus, generating CD4 and CD8 T cells. Naïve T cells are activated by their cognate Ag presented by mature DCs, they proliferate (blasts) in the SLO (LN, spleen, Peyer's patches (PP)) and differentiate into effector ($T_{EFF}$) or central memory T cells ($T_{CM}$) (see Supplemental **Table 1**. Follow the Supplemental Material link from the Annual Reviews home page at **http://www.annualreviews.org**). $T_{EFF}$ can either die or further differentiate to effector memory T cells ($T_{EM}$). $T_{EM}$ can differentiate in vivo into $T_{CM}$. $T_{CM}$ give rise to $T_{EFF}$ upon re-encounter with their Ag. Conversely, naïve B cells are activated in a T cell-dependent or -independent fashion (depending on the Ag); they proliferate in SLO (blasts) and give rise to plasma and memory B cells. Memory B cells can differentiate into plasma cells when re-encountering their Ag. DCs differentiate from lymphoid or myeloid progenitors (MP). Immature plasmacytoid DCs (i-pDC; found in blood and SLO) or immature conventional DCs (i-DC; found in blood an peripheral tissues) differentiate into mature DCs (m-pDC or m-DC) when encountering appropriate environmental signals (usually from pathogens) and then migrate into secondary lymphoid organs where they activate naïve T cells. Ag: antigen(s); TLR: Toll-like receptors.

Ag. The anatomic compartments where naïve lymphocytes encounter Ag are the SLO (e.g., spleen, LN, and Peyer's patches). These structures have evolved specialized mechanisms to collect Ag and Ag-presenting cells from peripheral tissues or (in case of the spleen) from the blood. Therefore, SLO represent the staging ground for adaptive immune responses, which involve a choreographed series of interactions between lymphocytes and DCs. IVM has been performed in various SLO (**Table 1**), but most published studies have focused on peripheral LN (PLN) and Peyer's patch.

**IVM models of peripheral lymph node and Peyer's patch for intravascular imaging.** At steady state, LN contain mostly naïve T and B lymphocytes, which are concentrated within the deep paracortex and the superficial cortical B cell follicles, respectively (**Figure 2**). Lymphocyte recruitment to LN occurs in specialized microvessels, the high endothelial venules (HEV), and involves a classic multistep adhesion cascade (Butcher & Picker 1996, von Andrian & Mackay 2000). The first IVM studies of SLO in mice were performed in exteriorized small intestine Peyer's patch (Bargatze et al. 1995) and in the subiliac LN (von Andrian 1996), which is surgically exposed by carefully dissecting and stabilizing an abdominal skin flap.

IVM studies have been instrumental in characterizing the various adhesion molecules involved in lymphocytes homing to PLN (reviewed in von Andrian & Mempel 2003) and Peyer's patch (Bargatze et al. 1995, Okada et al. 2002). In peripheral LN, the initial adhesive interaction requires binding of L-selectin on lymphocyte microvilli to HEV-expressed sulfated Lewis x ($sLe^x$) glycoproteins, collectively termed peripheral node addressin (PNAd). The unique kinetics of these lectin-carbohydrate interactions allow leukocytes to tether and roll slowly within HEV, even at high shear flow. Subsequently, the rolling lymphocytes are exposed to chemokines that are non-covalently presented on the luminal surface of HEV and activate chemokine receptors [CCR7 on T cells, CCR7 or CXCR4 (or possibly CXCR5) on B cells]. The latter then trigger activation of the lymphocyte-expressed integrin LFA-1, which mediates firm arrest by engaging with HEV-expressed ICAM-1 or ICAM-2 (von Andrian & Mempel 2003). By contrast, Peyer's patch HEV do not express PNAd in their lumen, but mucosal addressin cell-adhesion molecule 1 (MAdCAM-1), which binds the lymphocyte integrin $\alpha_4\beta_7$. Rolling of lymphocytes in Peyer's patch HEV is mediated by both L-selectin and $\alpha_4\beta_7$ interacting with different domains of MAdCAM-1 (Bargatze et al. 1995, Berg et al. 1993). Firm arrest of rolling lymphocytes in Peyer's patch HEV requires CCR7 for T cells, whereas some B cells can alternatively use CXCR4 and CXCR5 (Okada et al. 2002).

**Life within a lymph node: two-photon microscopy.** Two different LN in mice have been employed for 2P-IVM. The inguinal LN model used in intravascular IVM (von Andrian 1996) has been adapted to 2P-IVM (Lindquist et al. 2004, Miller et al. 2003b): This preparation requires mechanical restraints applied to the surrounding soft tissue to inhibit sample movement. More recently, the popliteal LN behind the knee has been used (Mempel et al. 2004). This model employs skeletal pivots as fixation points for near-perfect immobilization without application of force to soft tissue, which may interfere with lymph flow. Moreover, the T cell area is more superficial in the smaller popliteal node and is more accessible to deep imaging. Both LN preparations have yielded similar measurements of DC migration (Lindquist et al. 2004, Mempel et al. 2004) and T cell motility (Mempel et al. 2004, Miller et al. 2003b). The in vivo measurements of cell migration and communication are also in good agreement with 2PM studies performed in vitro in excised, intact murine LN (Miller et al. 2002, 2004a; Stoll et al. 2002). However, such ex vivo imaging studies require an environment containing 95% $O_2$, and it is not yet clear whether this non-physiologic

atmosphere and/or the absence of innervation, lymph, and blood flow affect cellular functions at a more subtle level.

Immunohistochemical analysis of histological sections have been instrumental in defining the different lymphocyte compartments in LN (**Figure 2**): B cells reside in subcapsular follicles, whereas T cells inhabit the deep cortex and the regions between and below B follicles called the cortical ridge, which also harbors a network of DCs (Lindquist et al. 2004). The medulla contains many lymphatic sinusoids and various macrophages, memory B cells, and plasma cells. Fibroblastic reticular cells (FRCs) form a meshwork throughout the cortex and are intimately associated with a web of collagen-rich extracellular matrix fibers that direct an ultra-filtrate of lymph from the subcapsular sinus to DCs in the T cell area (Gretz et al. 2000, Sixt et al. 2005). 2PM techniques, such as second harmonic generation of UV photons by collagen fibers, allow visualization of some of these fibers without specific staining (von Andrian & Mempel 2003). Putative gradients of chemokines and other factors that may affect cellular traffic and mobility in LN have not been visualized to date. In fact, it is currently unclear if such gradients really exist because thus far the migratory behavior of all observed intranodal leukocytes is best described as a random walk (Mempel et al. 2004, Miller et al. 2002).

**Watching the dance: T cell-dendritic cell interactions.** DCs are uniquely capable of both activating and inducing tolerance in naïve T cells (Banchereau et al. 2000, Steinman et al. 2003). Numerous DC subpopulations have been described in the mouse (Itano & Jenkins 2003). Most DCs arrive in LN via lymphatics that drain peripheral tissues. Several 2P-IVM studies have reported on DC motility and interactions with T cells in LN (Bousso & Robey 2003, Hugues et al. 2004, Lindquist et al. 2004, Mempel et al. 2004, Miller et al. 2004b, Stoll et al. 2002). Three primary means are known by which DCs acquire Ag for presentation in LN (Itano et al. 2003): (*a*) Soluble Ag in afferent lymph drains into the subcapsular sinus, where DCs can take up, process, and then carry Ag into the T cell area. (*b*) Alternatively, lymph-borne molecules with a radius of $\leq$4 nm can enter the FRC conduits and are acquired by resident DCs in the deep cortex (Sixt et al. 2005). (*c*) Finally, peripheral DCs endocytose or phagocytose Ag and, upon maturation, migrate via lymphatics into draining LN. 2P-IVM indicates that the latter DCs are initially more motile than their LN-resident counterparts, which are organized in relatively stationary networks (Lindquist et al. 2004). However, all DCs constantly extend and retract rapidly moving dendrites or lamellipodia, which contact large numbers of lymphocytes surrounding them. Estimates of the average rate of contacts between a DC and T cells ranges from 500–5000/h (Bousso & Robey 2003, Miller et al. 2004b). This may explain how a few Ag-bearing DCs can rapidly be detected by the rare T cells expressing a suitable TCR among the vast, highly diverse T cell pool.

Several studies using 2P-IVM have analyzed the quality and duration of T cell–DC interactions in LN and established that priming of both $CD8^+$ (Hugues et al. 2004, Mempel et al. 2004) and $CD4^+$ T cells (Miller et al. 2004b) occurs in distinct sequential stages: During the first 8 h upon entering the T cell area, T cells engage in multiple short-lasting contacts with DCs (phase 1). This is followed by a period of $\sim$12 h (phase 2) when T cells and DCs form long-lasting (>1 h) stable conjugates and begin to secrete cytokines. Finally, these conjugates dissociate, and T cells proliferate vigorously and resume their rapid migration while undergoing only brief interactions with DCs (phase 3).

DC-T cell interactions have mostly been analyzed during priming, but one recent report has also observed interactions during tolerance–induction (Hugues et al. 2004). Under these conditions, naïve T cells engaged in brief contacts with DCs but never entered

into stable interactions. Thus the duration and nature of T cell-DC contacts during phase 2 is probably critical for the outcome of immune responses.

**Homing preferences of antigen-experienced T cells.** Once naïve T cells have become activated in SLO, they proliferate and differentiate. Depending on the strength of the signal they receive through their TCR, and on the effect of local cytokines, T cells differentiate into various specialized effector cells ($T_{EFF}$) and into the longer-lived effector memory cells ($T_{EM}$) and central memory cells ($T_{CM}$) (Sallusto et al. 2004). $T_{EFF}$ were initially defined as CCR7$^-$L-selectin$^-$ memory marker–expressing cells that exert immediate effector/cytotoxic activity without the need for costimulation (see Supplemental **Table 1**. Follow the Supplemental Material link from the Annual Reviews home page at **http://www.annualreviews.org**) (Sallusto et al. 2004). In contrast, $T_{CM}$ were CCR7$^+$L-selectin$^+$ cells without immediate effector/cytotoxic activity, which proliferated and secreted cytokines, such as IL-2, more readily in response to recall Ag compared with naïve T cells or $T_{EFF}$ (Manjunath et al. 2001, Sallusto et al. 2004). However, virus-specific $T_{CM}$ in virally infected mice were shown to possess immediate effector activity comparable to that of $T_{EFF}$ or $T_{EM}$ (Gourley et al. 2004). In the mouse, $T_{EM}$ have been shown to convert slowly into a $T_{CM}$ phenotype expressing L-selectin and CCR7. Given their high expression of these trafficking molecules, $T_{CM}$ readily home into LN, whereas $T_{EFF}$ and $T_{EM}$ cannot access LN from the blood (Weninger et al. 2001). Some $T_{CM}$ also express adhesion molecules for migration into non-lymphoid tissues, such as the gut and the skin (Campbell et al. 2001), and both $T_{CM}$ and $T_{EM}$ (but not naïve T cells) migrate to acutely inflamed tissues (Weninger et al. 2001).

The small number of endogenous Ag-specific T cells that typically can be isolated from mice has limited their study by IVM. To bypass this difficulty, protocols for the in vitro generation and expansion of the different Ag-experienced T cell subpopulations have recently been established. For example, our laboratory has described that Ag-stimulated lymphoblasts cultured in the presence of IL-15, IL-7, or low doses of IL-2 acquire the phenotype and function of $T_{CM}$, whereas culture in high concentrations of IL-2 (>20 ng/ml) drives these cells to acquire phenotypic and functional properties of $T_{EFF}$ cells (**Figure 4**) (Manjunath et al. 2001). This simple approach has been exploited to produce the prerequisite numbers of effector/memory subsets for in vivo homing experiments and IVM (Mazo et al. 2005, Scimone et al. 2004, Weninger et al. 2001). These studies have demonstrated that in vitro–generated $T_{CM}$ migrate preferentially to SLO and the BM, whereas $T_{EFF}$ accumulate in certain extralymphoid tissues, such as liver and lung, and efficiently migrate to sites of inflammation (Weninger et al. 2001). However, neither ex vivo–generated $T_{CM}$ nor $T_{EFF}$ migrate to intestinal compartments. As is discussed below, T cells need additional tissue-specific imprinting signals to acquire gut-specific homing molecules.

**Tissue-specific T cell migration and differentiation.** DC from gut-associated lymphoid tissues imprint gut-homing potential on T cells upon activation (Iwata et al. 2004, Johansson-Lindbom et al. 2003, Mora et al. 2003). Conversely, non-gut associated DC from the spleen or cutaneous LN preferentially induce skin-homing T cells (Mora et al. 2005). Interestingly, gut- and skin-homing potentials of T cells represent dynamic functional states that can be rapidly modified when tissue-tropic memory T cells are restimulated in a different anatomic context (Mora et al. 2005). Recent evidence points to retinoic acid (RA), a vitamin A metabolite, as a central mediator in the imprinting of gut-homing T cells, and in fact gut-associated DCs, but not DCs from other SLO, express enzymes to convert food-derived vitamin A

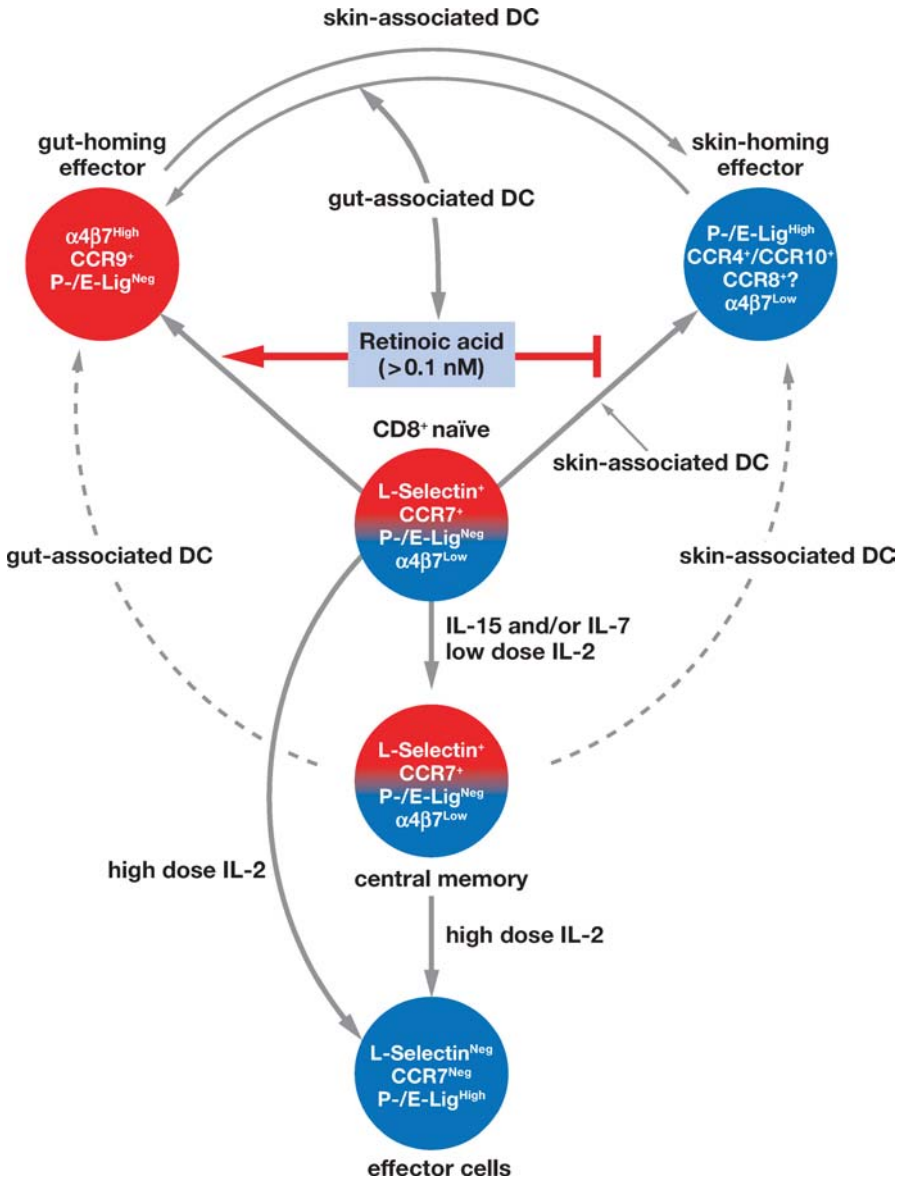


**Figure 4**

Ex vivo–generated gut- and skin-homing T cells and effector ($T_{EFF}$) and central memory ($T_{CM}$) $CD8^+$ T cells. To generate gut- or skin-homing T cells, naïve TCR–transgenic T cells are co-cultured during 4 to 5 days with Ag-pulsed PP- or PLN-DCs, respectively. Alternatively, T cells can be activated with plate-bound anti-CD3 + anti-CD28 in the presence or absence of *all-trans* retinoic acid (>0.1 nM), which generates gut- or skin-homing T cells, respectively. To generate $T_{EFF}$ and $T_{CM}$ $CD8^+$ T cells, total splenocytes from TCR transgenic mice are cultured for 2 h with the specific peptide, followed by 2 days without it. T cells are then cultured for 5 to 7 days in high-dose IL-2 (>20 ng/ml) to generate $T_{EFF}$, or in IL-15 and/or IL-7 (>5 ng/ml), or in low-dose IL-2, to obtain $T_{CM}$. Interestingly, gut- and skin-homing $CD8^+$ T cells can be significantly reversed in vitro by re-activating the effector T cells with the opposite DCs. Furthermore, ex vivo generated $T_{CM}$ can be differentiated into gut- or skin-homing effector T cells by re-activating them with PP- or PLN-DC, respectively.

into RA (Iwata et al. 2004). Conversely, the induction of E- and P-selectin ligands for skin-homing appears to be a default pathway in T cells activated in the absence of RA or gut-DCs (**Figure 4**) (Iwata et al. 2004, Mora et al. 2005).

Consequently, T cells activated by intestinal DCs roll poorly in skin-associated postcapillary venules, which constitutively express P- and E-selectin (Weninger et al. 2000) but not the $\alpha_4\beta_7$ ligand MAdCAM-1. By contrast, effector cells activated by DCs from non-intestinal SLO roll in skin-associated venules at a higher frequency and lower velocity than gut-tropic T cells and accumulate to significantly large numbers in inflamed skin (Mora et al. 2005).

**B cells and plasma cells.** Some information has also been gathered on the trafficking of B cell subsets (Kunkel & Butcher 2003). B-1 B cells constitute a small subset with self-renewal capacity and reside primarily in the abdominal and thoracic cavities where they continuously secrete low affinity "natural antibodies" (Poletaev & Osipenko 2003). By contrast, conventional naïve B cells (B-2 cells) become activated by Ag in a T cell–dependent or –independent fashion in SLO. B-2 cells subsequently differentiate into antibody-secreting cells (plasma cells) and migrate via the blood to spleen, BM (mainly IgG-producing plasma cells), or mucosal tissues (IgA-producing cells). Similarly to T cells, B cell-derived plasma cells also demonstrate tissue–tropism, depending on the site of B cell activation (Kunkel & Butcher 2003). B cells activated in gut-associated lymphoid tissues upregulate $\alpha_4\beta_7$ and CCR9 and/or CCR10, which target them to mucosal sites (Kunkel & Butcher 2003). To date, no IVM studies have been performed with Ag-experienced B cells. Although gut-DCs and RA apparently induce IgA isotype switching in B cells upon activation (Spalding et al. 1984, Tokuyama & Tokuyama 1996), it is unknown if these factors also induce gut-tropism in B cells. If this were the case, this could greatly facilitate the in vitro generation of gut-tropic plasma cells for use in IVM.

**IVM models for imaging lymphocytes in peripheral tissues.** Non-lymphoid tissues harbor the majority of early memory T lymphocytes that arise after systemic Ag challenge (Masopust et al. 2001, Reinhardt et al. 2001). These tissues must also recruit effector and memory lymphocytes generated in SLO in response to Ag challenge at a peripheral site. Indeed, effector cell recruitment is essential for lymphocytes to exert most of their protective and/or pathogenic activity. Some peripheral tissues (i.e., gut and skin) can recruit lymphocytes under non-inflammatory steady-state conditions because their microvessels constitutively express tissue-specific adhesion molecules and chemokines for homeostatic recruitment. In addition, all tissues can recruit lymphocytes upon induction by inflammatory signals, which upregulate a plethora of adhesion molecules recognized by most effector cells. 2P-IVM studies of interstitial lymphocyte migration in non-lymphoid tissues have been initiated only recently, but several epifluoresence-based IVM studies have already characterized the intravascular lymphocyte recruitment steps in such tissues under both non-inflammatory and inflammatory conditions. A representative (but invariably incomplete) selection of relevant examples in the mouse is briefly discussed below:

***Skin.*** The skin is the body's most vulnerable organ and consequently requires specialized mechanisms of immune surveillance for protection against external hazards (Kupper & Fuhlbrigge 2004). IVM of the mouse ear microcirculation allows percutaneous observations of leukocyte adhesion in dermal microvessels without requiring surgical manipulation (Reus et al. 1984). The model has been valuable for studying physiologic cutaneous immune surveillance, in particular with regard to P- and E-selectin and the leukocyte-expressed glycoproteins and

glycosyltransferases that contribute to selectin ligand activity (Maly et al. 1996, Weninger et al. 2000). Moreover, the skin is the target of acute and chronic inflammation. However, inflammatory events are difficult to visualize in the ear model because the intact epidermis impedes experimental application of many pro-inflammatory reagents, and inflammation-induced tissue swelling reduces visibility of dermal microvessels. Other IVM models that visualize dermal and subdermal microvessels, such as the dorsal skinfold chamber preparation, may be more suitable for studying inflamed skin (Lehr et al. 1994).

***Cremaster muscle.*** The murine cremaster muscle consists of a thin sheet of striated muscle cells that surround the testis and is easily exposed. This tissue has been the prototypical peripheral site to perform IVM under acute inflammatory conditions (Baez 1973, Ley et al. 1995). The model features excellent optical properties, access to a dense, highly organized network of microvessels, and the possibility for easy experimental manipulation such as exposure to inflammatory mediators.

***Small and large intestine.*** One IVM model to image the intestinal microvasculature has been described (Fujimori et al. 2002). It involves exteriorizing an intestinal loop and opening the intestine for visualization of microvessels from the luminal mucosal surface. This technique has so far not been employed to image highly dynamic events, such as lymphocyte tethering and rolling. A technical challenge for IVM of intestinal microvasculature is the intrinsic, peristaltic tissue movement, which can deteriorate the quality of IVM recordings, especially at high magnification. This latter problem could be alleviated by local drug treatment (e.g., with atropine).

***Liver.*** The liver IVM model has been used to obtain unique insights into leukocyte and platelet interactions with highly specialized hepatic microvessels and intrahepatic macrophages, respectively (Hoffmeister et al. 2003, Nakagawa et al. 1996). A major technical difficulty of this model is reducing the breathing-associated movement of the liver to allow precise imaging. This problem is more acute with upright microscopes when imaging the liver from above. Using an inverted setup, the liver's own weight helps keep the tissue still and in focus, albeit at the expense of easy access to the tissue for rapid experimental manipulation.

***Central nervous system.*** Three different models have been described for visualizing intravascular adhesion events in the central nervous system (CNS). A simple model exists for imaging brain microvessels in anaesthetized mice, by exposing the scalp in the parietal area where bones are sufficiently transparent for direct imaging of underlying superficial brain microvessels (Piccio et al. 2002). Furthermore, a cranial window model also exists (Yuan et al. 1994). These models have been used for studying T cell interactions with cortical venules under steady-state and inflammatory conditions. A technically more challenging approach is IVM of spinal cord microvessels, which requires sophisticated microsurgical techniques (Vajkoczy et al. 2001) but allows unique insight to elucidate the adhesion pathways involved in the recruitment of T cells to both the gray and white matter of the CNS.

## TECHNICAL CONSIDERATIONS

Most questions in biology cannot be addressed experimentally without inflicting some degree of manipulation on the system under study. In IVM, these manipulations comprise the use of anesthetics and other drugs, invasive surgical procedures to expose tissues, purification and fluorescent labeling of cells, and tissue exposure to intense illumination causing potential phototoxicity. The manual or computer-assisted analysis of

complex imaging data sets also represents a possible source of errors. To obtain IVM data that describe in vivo leukocyte behavior accurately, it is important to recognize possible caveats and to take appropriate precautions.

## Surgical Preparation and Associated Issues

Most IVM models require tissue dissection to create optimal accessibility for imaging. This procedure likely induces local or systemic inflammation. Several measures can keep inflammation to a minimum: Surgical equipment and buffer solutions must be free of contamination with bacteria or bacterial byproducts (e.g., endotoxins); drying of exposed tissue must be prevented to avoid thrombosis, inflammation and cell necrosis; proper surgical techniques also require careful dosage of anesthetics for full analgesia without causing hypotension or respiratory depression; the temperature of the animal and the exposed tissue should be monitored because interstitial cell motility is compromised below 35°C (Miller et al. 2002).

IVM typically requires specialized stages for optimally positioning and immobilizing the animal. This is particularly important for three-dimensional imaging using 2P-IVM. Lymphocytes in tissue move two to three orders of magnitude more slowly than in microvessels (a few micrometers per minute compared with several millimeters per second for cells in arterioles). Thus, to accurately detect interstitial cell movement, long observation periods (up to hours) are needed to obtain three-dimensional information from stacks of multiple optical sections, which must be acquired over scan intervals lasting up to 1 min each (**Figure 1*b***). Tissue movement by as little as a few micrometers can render three-dimensional image stacks uninterpretable (imagine holding a camera with a 1-min shutter speed). Conversely, application of mechanical force to immobilize the tissue must not interfere with physiologic functions such as lymph and blood flow.

## Cell Purification

Intravascular IVM with ex vivo purified and fluorescently labeled cells requires that the cells be re-introduced into the circulation. To minimize cell loss in the circulation upon i.v. injection, cells are ideally injected directly into an artery upstream of the tissue under observation. Even so, intravascular IVM generally requires several million highly purified cells—a number difficult to obtain for rare primary cell types. Cell lines are often not a viable alternative because many long-term cultured cells are much larger than blood-borne leukocytes and can cause massive capillary plugging upon i.v. injection, sometimes with lethal consequences. When using fluorescently tagged primary cells, high purity is essential because contaminating cells will not be distinguishable. Additionally, cell purification and fluorescent labeling may damage or otherwise alter the cells. The latter concern especially holds true for DCs, which are easily induced to mature, but improper ex vivo handling can also affect other leukocytes, e.g., by inducing shedding of L-selectin or increasing apoptosis. The quality of purified and labeled cells should, therefore, be monitored in parallel assays, such as quantitative homing studies, chemotaxis experiments, or flow cytometry.

## Data Acquisition, Analysis, and Interpretation

Compared with intravascular video-based epifluorescence IVM, three-dimensional imaging within living tissue is a very young discipline and, consequently, still faces many unresolved technical issues. Primarily, the transition from two-dimensional imaging of cells within vessels to three-dimensional imaging of cells moving freely in any direction adds considerable complexity to both imaging and analysis.

For example, T cell motility varies between shallow and deep T cell areas (relative to the capsule) of the same LN. Thus to compare results from different experiments, it is important to consider imaging depth and anatomic location (Mempel et al. 2004, Stoll et al. 2002). Furthermore, non-fluorescent structures such as unlabeled cells, connective tissue fibers, blood vessels, or lymphatics may influence cell motility. Lastly, highly motile cells may be over-represented in certain measurements as they may transiently leave a scanned volume of tissue and then re-enter it to be counted as a new cell.

Clearly, the unique challenges and limitations of three-dimensional imaging of the immune system in a living animal are only now beginning to be understood and will take some time to be adequately addressed. Similarly, at the level of data processing and presentation, substantial variability exists between the approaches undertaken by different research teams. Therefore, it will be important that measurement parameters are clearly defined and that investigators in the field agree on common procedures to generate a better understanding of the relevance of different measurement parameters.

## LITERATURE CITED


Atherton A, Born GVR. 1972. Quantitative investigation of the adhesiveness of circulating polymorphonuclear leucocytes to blood vessel walls. *J. Physiol.* 222:447–74

Baez S. 1973. An open cremaster muscle preparation for the study of blood vessels by in vivo microscopy. *Microvasc. Res.* 5:384–94

Banchereau J, Briere F, Caux C, Davoust J, Lebecque S, et al. 2000. Immunobiology of dendritic cells. *Annu. Rev. Immunol.* 18:767–811

Bargatze RF, Jutila MA, Butcher EC. 1995. Distinct roles of L-selectin and integrins $\alpha$ 4$\beta$ 7 and LFA-1 in lymphocyte homing to Peyer's patch-HEV in situ: the multistep model confirmed and refined. *Immunity* 3:99–108

Becker MD, Nobiling R, Planck SR, Rosenbaum JT. 2000. Digital video-imaging of leukocyte migration in the iris: intravital microscopy in a physiological model during the onset of endotoxin-induced uveitis. *J. Immunol. Methods* 240:23–37

Berg EL, McEvoy LM, Berlin C, Bargatze RF, Butcher EC. 1993. L-selectin-mediated lymphocyte rolling on MAdCAM-1. *Nature* 366:695–98

Bhakta NR, Oh DY, Lewis RS. 2005. Calcium oscillations regulate thymocyte motility during positive selection in the three-dimensional thymic environment. *Nat. Immunol.* 6:143–51

Bousso P, Bhakta NR, Lewis RS, Robey E. 2002. Dynamics of thymocyte-stromal cell interactions visualized by two-photon microscopy. *Science* 296:1876–80

Bousso P, Robey E. 2003. Dynamics of $CD8^+$ T cell priming by dendritic cells in intact lymph nodes. *Nat. Immunol.* 4:579–85

Butcher EC, Picker LJ. 1996. Lymphocyte homing and homeostasis. *Science* 272:60–66

Cahalan MD, Parker I, Wei SH, Miller MJ. 2002. Two-photon tissue imaging: seeing the immune system in a fresh light. *Nat. Rev. Immunol.* 2:872–80

Calvi LM, Adams GB, Weibrecht KW, Weber JM, Olson DP, et al. 2003. Osteoblastic cells regulate the haematopoietic stem cell niche. *Nature* 425:841–46

Campbell JJ, Murphy KE, Kunkel EJ, Brightling CE, Soler D, et al. 2001. CCR7 expression and memory T cell diversity in humans. *J. Immunol.* 166:877–84

Cohnheim J. 1889. *Lectures on General Pathology: A Handbook for Practitioners and Students*. London: New Sydenham Society

Denk W, Strickler JH, Webb WW. 1990. Two-photon laser scanning fluorescence microscopy. *Science* 248:73–76

Di Rosa F, Santoni A. 2002. Bone marrow CD8 T cells are in a different activation state than those in lymphoid periphery. *Eur. J. Immunol.* 32:1873–80

Enghofer M, Bojunga J, Usadel KH, Kusterer K. 1995. Intravital measurement of donor lymphocyte adhesion to islet endothelium of recipient animals in diabetes transfer experiments. *Exp. Clin. Endocrinol. Diabetes* 103(Suppl.) 2:99–102

Feuerer M, Beckhove P, Garbi N, Mahnke Y, Limmer A, et al. 2003. Bone marrow as a priming site for T-cell responses to blood-borne antigen. *Nat. Med.* 9:1151–57

Feuerer M, Beckhove P, Mahnke Y, Hommel M, Kyewski B, et al. 2004. Bone marrow microenvironment facilitating dendritic cell: CD4 T cell interactions and maintenance of CD4 memory. *Int. J. Oncol.* 25:867–76

Fujimori H, Miura S, Koseki S, Hokari R, Komoto S, et al. 2002. Intravital observation of adhesion of lamina propria lymphocytes to microvessels of small intestine in mice. *Gastroenterology* 122:734–44

Gesner BM, Gowans JL. 1962. The output of lymphocytes from the thoracic duct of unanaesthetized mice. *Br. J. Exp. Pathol.* 43:424

Gourley TS, Wherry EJ, Masopust D, Ahmed R. 2004. Generation and maintenance of immunological memory. *Semin. Immunol.* 16:323–33

Grayson MH, Hotchkiss RS, Karl IE, Holtzman MJ, Chaplin DD. 2003. Intravital microscopy comparing T lymphocyte trafficking to the spleen and the mesenteric lymph node. *Am. J. Physiol. Heart Circ. Physiol.* 284:H2213–26

Gretz JE, Norbury CC, Anderson AO, Proudfoot AE, Shaw S. 2000. Lymph-borne chemokines and other low molecular weight molecules reach high endothelial venules via specialized conduits while a functional barrier limits access to the lymphocyte microenvironments in lymph node cortex. *J. Exp. Med.* 192:1425–40

Haddad W, Cooper CJ, Zhang Z, Brown JB, Zhu Y, et al. 2003. P-selectin and P-selectin glycoprotein ligand 1 are major determinants for Th1 cell recruitment to nonlymphoid effector sites in the intestinal lamina propria. *J. Exp. Med.* 198:369–77

Hoffmeister KM, Felbinger TW, Falet H, Denis CV, Bergmeier W, et al. 2003. The clearance mechanism of chilled blood platelets. *Cell* 112:87–97

Hosoe N, Miura S, Watanabe C, Tsuzuki Y, Hokari R, et al. 2004. Demonstration of functional role of TECK/CCL25 in T lymphocyte-endothelium interaction in inflamed and uninflamed intestinal mucosa. *Am. J. Physiol. Gastrointest. Liver Physiol.* 286:G458–66

Hugues S, Fetler L, Bonifaz L, Helft J, Amblard F, Amigorena S. 2004. Distinct T cell dynamics in lymph nodes during the induction of tolerance and immunity. *Nat. Immunol.* 5:1235–42

Itano AA, Jenkins MK. 2003. Antigen presentation to naïve CD4 T cells in the lymph node. *Nat. Immunol.* 4:733–39

Itano AA, McSorley SJ, Reinhardt RL, Ehst BD, Ingulli E, et al. 2003. Distinct dendritic cell populations sequentially present a subcutaneous antigen to CD4 T cells and stimulate different aspects of cell-mediated immunity. *Immunity* 19:47–57

Iwata M, Hirakiyama A, Eshima Y, Kagechika H, Kato C, Young SY. 2004. Retinoic acid imprints gut-homing specificity on T cells. *Immunity* 21(4):527–38

Johansson-Lindbom B, Svensson M, Wurbel MA, Malissen B, Marquez G, Agace W. 2003. Selective generation of gut tropic T cells in gut-associated lymphoid tissue (GALT): requirement for GALT dendritic cells and adjuvant. *J. Exp. Med.* 198:963–69

Katayama Y, Hidalgo A, Furie BC, Vestweber D, Furie B, Frenette PS. 2003. PSGL-1 participates in E-selectin-mediated progenitor homing to bone marrow: evidence for cooperation between E-selectin ligands and alpha4 integrin. *Blood* 102:2060–67

Katsura Y. 2002. Redefinition of lymphoid progenitors. *Nat. Rev. Immunol.* 2:127–32

Koni PA, Joshi SK, Temann UA, Olson D, Burkly L, Flavell RA. 2001. Conditional vascular cell adhesion molecule 1 deletion in mice. Impaired lymphocyte migration to bone marrow. *J. Exp. Med.* 193:741–54

Kunkel EJ, Butcher EC. 2003. Plasma-cell homing. *Nat. Rev. Immunol.* 3:822–29

Kupper TS, Fuhlbrigge RC. 2004. Immune surveillance in the skin: mechanisms and clinical consequences. *Nat. Rev. Immunol.* 4:211–22

Lakkis FG, Arakelov A, Konieczny BT, Inoue Y. 2000. Immunologic 'ignorance' of vascularized organ transplants in the absence of secondary lymphoid tissue. *Nat. Med.* 6:686–88

Lehr HA, Olofsson AM, Carew TE, Vajkoczy P, von Andrian UH, et al. 1994. P-selectin mediates the interaction of circulating leukocytes with platelets and microvascular endothelium in response to oxidized lipoprotein in vivo. *Lab. Invest.* 71:380–86

Leunig M, Yuan F, Menger MD, Boucher Y, Goetz AE, et al. 1992. Angiogenesis, microvascular architecture, microhemodynamics, and interstitial fluid pressure during early growth of human adenocarcinoma LS174T in SCID mice. *Cancer Res.* 52:6553–60

Ley K, Bullard DC, Arbonés ML, Bosse R, Vestweber D, et al. 1995. Sequential contribution of L- and P-selectin to leukocyte rolling in vivo. *J. Exp. Med.* 181:669–75

Lind EF, Prockop SE, Porritt HE, Petrie HT. 2001. Mapping precursor movement through the postnatal thymus reveals specific microenvironments supporting defined stages of early lymphoid development. *J. Exp. Med.* 194:127–34

Lindquist RL, Shakhar G, Dudziak D, Wardemann H, Eisenreich T, et al. 2004. Visualizing dendritic cell networks in vivo. *Nat. Immunol.* 5:1243–50

Lord BI, Testa NG, Hendry JH. 1975. The relative spatial distributions of CFUs and CFUc in the normal mouse femur. *Blood* 46:65–72

Maly P, Thall AD, Petryniak B, Rogers CE, Smith PL, et al. 1996. The $\alpha_{1,3}$ fucosyltransferase Fuc-TVII controls leukocyte trafficking through an essential role in L-, E-, and P-selectin ligand biosynthesis. *Cell* 86:643–53

Manjunath N, Shankar P, Stockton B, Dubey PD, Lieberman J, von Andrian UH. 1999. A transgenic mouse model to analyze $CD8^+$ effector T cell differentiation in vivo. *Proc. Natl. Acad. Sci. USA* 96:13932–37

Manjunath N, Shankar P, Wan J, Weninger W, Crowley MA, et al. 2001. Effector differentiation is not prerequisite for generation of memory cytotoxic T lymphocytes. *J. Clin. Invest.* 108:871–78

Masopust D, Vezys V, Marzo AL, Lefrancois L. 2001. Preferential localization of effector memory cells in nonlymphoid tissue. *Science* 291:2413–17

Massberg S, Enders G, Leiderer R, Eisenmenger S, Vestweber D, et al. 1998. Platelet-endothelial cell interactions during ischemia/reperfusion: the role of P-selectin. *Blood* 92:507–15

Matz MV, Fradkov AF, Labas YA, Savitsky AP, Zaraisky AG, et al. 1999. Fluorescent proteins from nonbioluminescent Anthozoa species. *Nat. Biotechnol.* 17:969–73

Mazo IB, Gutierrez-Ramos J-C, Frenette PS, Hynes RO, Wagner DD, von Andrian UH. 1998. Hematopoietic progenitor cell rolling in bone marrow microvessels: parallel contributions by endothelial selectins and VCAM-1. *J. Exp. Med.* 188:465–74

Mazo IB, Honczarenko M, Leung H, Cavanagh LL, Bonasio R, et al. 2005. Bone marrow is a major reservoir and site of recruitment for central memory $CD8^+$ T Cells. *Immunity* 22:259–70

Mazo IB, Quackenbush EJ, Lowe JB, von Andrian UH. 2002. Total body irradiation causes profound changes in endothelial traffic molecules for hematopoietic progenitor cell recruitment to bone marrow. *Blood* 99:4182–91

Mazo IB, von Andrian UH. 1999. Adhesion and homing of blood-borne cells in bone marrow microvessels. *J. Leukoc. Biol.* 66:25–32

Mempel TR, Henrickson SE, von Andrian UH. 2004. T cell priming by dendritic cells in lymph nodes occurs in three distinct phases. *Nature* 427:154–59

Michalet X, Pinaud FF, Bentolila LA, Tsay JM, Doose S, et al. 2005. Quantum dots for live cells, in vivo imaging, and diagnostics. *Science* 307:538–44

Miller DH, Khan OA, Sheremata WA, Blumhardt LD, Rice GP, et al. 2003a. A controlled trial of natalizumab for relapsing multiple sclerosis. *N. Engl. J. Med.* 348:15–23

Miller MJ, Hejazi AS, Wei SH, Cahalan MD, Parker I. 2004a. T cell repertoire scanning is promoted by dynamic dendritic cell behavior and random T cell motility in the lymph node. *Proc. Natl. Acad. Sci. USA* 101:998–1003

Miller MJ, Safrina O, Parker I, Cahalan MD. 2004b. Imaging the single cell dynamics of $CD4^+$ T cell activation by dendritic cells in lymph nodes. *J. Exp. Med.* 200:847–56

Miller MJ, Wei SH, Cahalan MD, Parker I. 2003b. Autonomous T cell trafficking examined in vivo with intravital two-photon microscopy. *Proc. Natl. Acad. Sci. USA* 100:2604–9

Miller MJ, Wei SH, Parker I, Cahalan MD. 2002. Two-photon imaging of lymphocyte motility and antigen response in intact lymph node. *Science* 296:1869–73

Mora JR, Bono MR, Manjunath N, Weninger W, Cavanagh LL, et al. 2003. Selective imprinting of gut-homing T cells by Peyer's patch dendritic cells. *Nature* 424:88–93

Mora JR, Cheng G, Picarella D, Briskin M, Buchanan N, von Andrian UH. 2005. Reciprocal and dynamic control of CD8 T cell homing by dendritic cells from skin- and gut-associated lymphoid tissues. *J. Exp. Med.* 201:303–16

Nakagawa K, Miller FN, Sims DE, Lentsch AB, Miyazaki M, Edwards MJ. 1996. Mechanisms of interleukin-2-induced hepatic toxicity. *Cancer Res.* 56:507–10

Nilsson SK, Johnston HM, Coverdale JA. 2001. Spatial localization of transplanted hemopoietic stem cells: inferences for the localization of stem cell niches. *Blood* 97:2293–99

Okada T, Ngo VN, Ekland EH, Forster R, Lipp M, et al. 2002. Chemokine requirements for B cell entry to lymph nodes and Peyer's patches. *J. Exp. Med.* 196:65–75

Patterson GH, Lippincott-Schwartz J. 2004. Selective photolabeling of proteins using photoactivatable GFP. *Methods* 32:445–50

Petrie HT. 2003. Cell migration and the control of post-natal T-cell lymphopoiesis in the thymus. *Nat. Rev. Immunol.* 3:859–66

Piccio L, Rossi B, Scarpini E, Laudanna C, Giagulli C, et al. 2002. Molecular mechanisms involved in lymphocyte recruitment in inflamed brain microvessels: critical roles for P-selectin glycoprotein ligand-1 and heterotrimeric $G_i$-linked receptors. *J. Immunol.* 168:1940–49

Poletaev A, Osipenko L. 2003. General network of natural autoantibodies as immunological homunculus (Immunculus). *Autoimmun. Rev.* 2:264–71

Reinhardt RL, Khoruts A, Merica R, Zell T, Jenkins MK. 2001. Visualizing the generation of memory CD4 T cells in the whole body. *Nature* 410:101–5

Reus WF, Robson MC, Zachary L, Heggers JP. 1984. Acute effects of tobacco smoking on blood flow in the cutaneous micro-circulation. *Br. J. Plast. Surg.* 37:213–15

Richie LI, Ebert PJ, Wu LC, Krummel MF, Owen JJ, Davis MM. 2002. Imaging synapse formation during thymocyte selection: inability of CD3zeta to form a stable central accumulation during negative selection. *Immunity* 16:595–606

Saetzler RK, Jallo J, Lehr HA, Philips CM, Vasthare U, et al. 1997. Intravital fluorescence microscopy: impact of light-induced phototoxicity on adhesion of fluorescently labeled leukocytes. *J. Histochem. Cytochem.* 45:505–13

Sallusto F, Geginat J, Lanzavecchia A. 2004. Central memory and effector memory T cell subsets: function, generation, and maintenance. *Annu. Rev. Immunol.* 22:745–63

Scimone ML, Felbinger TW, Mazo IB, Stein JV, von Andrian UH, Weninger W. 2004. CXCL12 mediates CCR7-independent homing of central memory cells, but not naive T cells, in peripheral lymph nodes. *J. Exp. Med.* 199:1113–20

Shinkura R, Matsuda F, Sakiyama T, Tsubata T, Hiai H, et al. 1996. Defects of somatic hypermutation and class switching in alymphoplasia (*aly*) mutant mice. *Int. Immunol.* 8:1067–75

Singbartl K, Thatte J, Smith ML, Wethmar K, Day K, Ley K. 2001. A CD2-green fluorescence protein-transgenic mouse reveals very late antigen-4-dependent $CD8^+$ lymphocyte rolling in inflamed venules. *J. Immunol.* 166:7520–26

Sixt M, Kanazawa N, Selg M, Samson T, Roos G, et al. 2005. The conduit system transports soluble antigens from the afferent lymph to resident dendritic cells in the T cell area of the lymph node. *Immunity* 22:19–29

Spalding DM, Williamson SI, Koopman WJ, McGhee JR. 1984. Preferential induction of polyclonal IgA secretion by murine Peyer's patch dendritic cell-T cell mixtures. *J. Exp. Med.* 160:941–46

Springer TA. 1994. Traffic signals for lymphocyte recirculation and leukocyte emigration: the multi-step paradigm. *Cell* 76:301–14

Steinman RM, Hawiger D, Nussenzweig MC. 2003. Tolerogenic dendritic cells. *Annu. Rev. Immunol.* 21:685–711

Stoll S, Delon J, Brotz TM, Germain RN. 2002. Dynamic imaging of T cell-dendritic cell interactions in lymph nodes. *Science* 296:1873–76

Sumen C, Mempel TR, Mazo IB, Von Andrian UH. 2004. Intravital microscopy; visualizing immunity in context. *Immunity* 21:315–29

Tietz W, Allemand Y, Borges E, von Laer D, Hallmann R, et al. 1998. $CD4^+$ T cells migrate into inflamed skin only if they express ligands for E- and P-selectin. *J. Immunol.* 161:963–70

Tokoyoda K, Egawa T, Sugiyama T, Choi BI, Nagasawa T. 2004. Cellular niches controlling B lymphocyte behavior within bone marrow during development. *Immunity* 20:707–18

Tokuyama Y, Tokuyama H. 1996. Retinoids as Ig isotype-switch modulators. *Cell. Immunol.* 170:230–34

Vajkoczy P, Laschinger M, Engelhardt B. 2001. Alpha4-integrin-VCAM-1 binding mediates G protein-independent capture of encephalitogenic T cell blasts to CNS white matter microvessels. *J. Clin. Invest.* 108:557–65

Verkhusha VV, Lukyanov KA. 2004. The molecular properties and applications of Anthozoa fluorescent proteins and chromoproteins. *Nat. Biotechnol.* 22:289–96

von Andrian UH. 1996. Intravital microscopy of the peripheral lymph node microcirculation in mice. *Microcirculation* 3:287–300

von Andrian UH, Mackay CR. 2000. T-cell function and migration. Two sides of the same coin. *N. Engl. J. Med.* 343:1020–34

von Andrian UH, Mempel TR. 2003. Homing and cellular traffic in lymph nodes. *Nat. Rev. Immunol.* 3:867–78

Vugmeyster Y, Kikuchi T, Lowes MA, Chamian F, Kagen M, et al. 2004. Efalizumab (anti-CD11a)-induced increase in peripheral blood leukocytes in psoriasis patients is preferentially mediated by altered trafficking of memory $CD8^+$ T cells into lesional skin. *Clin. Immunol.* 113:38–46

Wagner R. 1839. *Erläuterungstafeln zur Physiologie und Entwicklungsgeschichte*. Leipzig: Voss

Weninger W, Carlsen HS, Goodarzi M, Moazed F, Crowley MA, et al. 2003. Naïve T cell recruitment to non-lymphoid tissues: a role for endothelium-expressed CCL21 in autoimmune disease and lymphoid neogenesis. *J. Immunol.* 170:4638–48

Weninger W, Crowley MA, Manjunath N, von Andrian UH. 2001. Migratory properties of naive, effector, and memory $CD8^+$ T cells. *J. Exp. Med.* 194:953–66

Weninger W, Ulfman LH, Cheng G, Souchkova N, Quackenbush EJ, et al. 2000. Specialized contributions by $alpha_{1,3}$-fucosyltransferase-IV and FucT-VII during leukocyte rolling in dermal microvessels. *Immunity* 12:665–76

Yu W, Nagaoka H, Jankovic M, Misulovin Z, Suh H, et al. 1999. Continued RAG expression in late stages of B cell development and no apparent re-induction after immunization. *Nature* 400:682–87

Yuan F, Salehi HA, Boucher Y, Vasthare US, Tuma RF, Jain RK. 1994. Vascular permeability and microcirculation of gliomas and mammary carcinomas transplanted in rat and mouse cranial windows. *Cancer Res.* 54:4564–68

Zhang J, Campbell RE, Ting AY, Tsien RY. 2002. Creating new fluorescent probes for cell biology. *Nat. Rev. Mol. Cell. Biol.* 3:906–18

Zipfel WR, Williams RM, Webb WW. 2003. Nonlinear magic: multiphoton microscopy in the biosciences. *Nat. Biotechnol.* 21:1369–77

Annual Review of Cell and Developmental Biology

Volume 21, 2005



# Contents

INDEXES



ERRATA

An online log of corrections to *Annual Review of Cell and Developmental Biology* chapters may be found at http://cellbio.annualreviews.org/errata.shtml